Supporting Information for:

A superior compatible non-flammable electrolyte to hard carbon anode

for robust sodium ion batteries

Xuechun Huang[a], Xiaojuan Chen*[a], Yan Meng[b], Ruixiang Wang[a], Guangqun Tan*[a] and Dan Xiao[ab]

[a.] School of Chemical Engineering, Sichuan University, Chengdu 610065, (P. R. China)

[b.] Institute of New Energy and Low-Carbon Technology, Sichuan University, Chengdu, Sichuan, 610065, (P.R. China)

Experimental section:

Preparation of electrolyte and electrodes

The non-flammable electrolytes were prepared by mixing sodium hexafluorophosphate (NaFSI) (DODO chem,99.9%) with tris(2,2,2-trifluoroethyl) phosphate (TFEP) (Admas, 98%) (1:5 in mole) or trimethyl phosphate (TMP) (DODO chem, 99.8%) (0.92 M) in an Ar-filled glove box with O_2 and H_2O contents below 0.1 ppm. The commercial electrolytes for comparison are 1 M $NaPF_6$ in DEC/FEC (4:1 in volume DODO chem), 1 M $NaPF_6$/EC+DEC (1:1 in volume) with 5% vol FEC and 1 M $NaClO_4$/EC+DEC (1:1 in volume) with 5% vol FEC. All the solvents and electrolytes were dried by molecular sieve before use.

Commercial hard carbon powder was purchased from Kuraray (Type Ⅱ), and was dried at 100 °C for a week before use. The HC electrodes were prepared by mixing with super p and PVDF (Sigma-Aldrich), with a mass ratio of 90:5:5 (HC: super p: PVDF) in N-methyl-2-pyrrolidinone (NMP) solvent followed by doctor blading on carbon coated Al foil. The HC electrodes were punched into small disks with a diameter of 12 mm and dried under vacuum at 100 °C before use. The final mass loading of active material is about 1.5 mg cm^{-1}.

Electrochemical measurements

The electrochemical performance and Na$^+$ storage mechanism of the working electrodes in different electrolytes were evaluated using a 2032 type button cell with Na metal (Xiya Reagent, 99%) as the reference electrode and a hard carbon as the working electrode, using glass fiber (GF-A, Whatman) and Celgard-2500 as the diaphragm, and 80 μL electrolyte was added to each cell. Constant current tests were performed using a Neware battery test system (CT-4008T-5V20mA-164) with a voltage range of 0.01-2 V (vs. Na/Na$^+$). The linear scanning voltammetry (LSV) and cyclic voltammetry (CV) were performed on a PARSTAT 3000A DX system (Princeton) in a two-electrode system at a scan rate of 0.1 mV s^{-1}. The in-situ EIS tests of the Na/HC half-cells were determined in the range of 10^5-1 Hz with an amplitude of 2 mV s^{-1} and an impedance acquisition interval of 703 s. The conversion of the raw impedance data into DRTs was performed by the Matlab GUI toolbox developed by Ciucci's team.[1] The room-temperature ionic conductivity of NaFSI/TFEP and NP003 was measured with the DDS-11A Conductivity Meter (Shanghai Lei-Ci) with the value of 0.314 mS cm^{-1} and 5.01 mS cm^{-1}, respectively.

Characterizations

200 μL electrolyte was introduced in the cathode shell and evaluated for its combustion performance under ambient conditions. The solvation structure of the electrolytes was characterized in Raman using a microscope (HORIBA LabRAM Soleil, Japan) with a 532 nm excitation laser, while X-ray photoelectron spectroscopy (Thermo Scientific K-Alpha) was used to

investigate the interfacial chemistry of the passivation layer on the hard carbon surface. The SEI thickness on cycled HC electrodes were tested with high-resolution transmission microscopy (HR-TEM) (JEOL, JEM-F200, 20236135) with the samples scratched from HC electrode surface and rinsed with DEC solvent.

Computational details

Molecular Dynamics (MD) simulation and Density Functional Tolerance (DFT) calculations of solvation structures were carried out in Materials Studio. The solvation structure of electrolyte was modelled using the Amorphous Cell (AC) module. Then the structural optimization and kinetic calculations were carried out in the Forcite module with COMPASS III as force field. The radial distribution function and the coordination number information were obtained from the kinetic calculations carried out using NVT followed by NPT.[2] DFT calculations were performed in the Dmol3 module[3, 4], using the electron exchange correlation potential using the BLYP functional of the generalized gradient approximation (GGA) to complete the structure optimization and energy calculations, with a DNP basis group, a self-consistent field energy convergence criterion of 1×10^{-6} eV/atom, and orbital occupancy values of 0.01 Ha. The electrostatic potential (ESP) was calculated by the DFT[5] at the b3lyp/6-31+G(d) level[6] by Gaussian16 program[7]. Related images were drawn with Multiwfn and VMD together.[8,9]
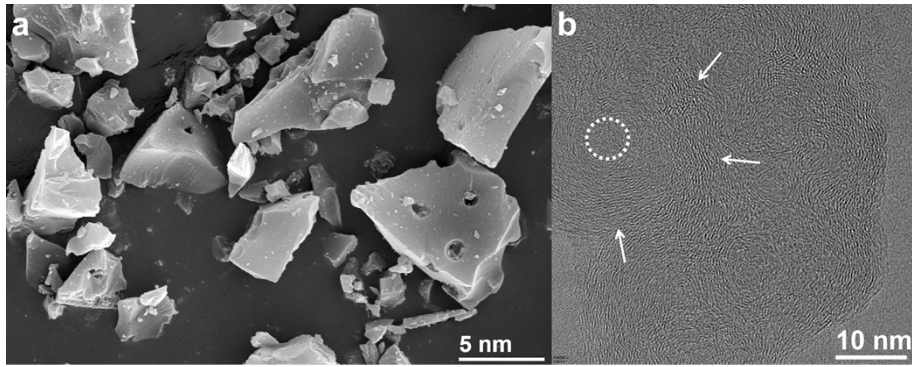
Fig. S1 (a) SEM and (b) TEM images of pristine HC.

It can be seen that hard carbon has a structure with the appearance of disordered lamellar structures in the scanning electron microscope (SEM) (Fig. S1a). Whereas the characteristic structures of long-range disorder and short-range order are clearer in transmission electron microscopy (TEM) (Fig. S1b).
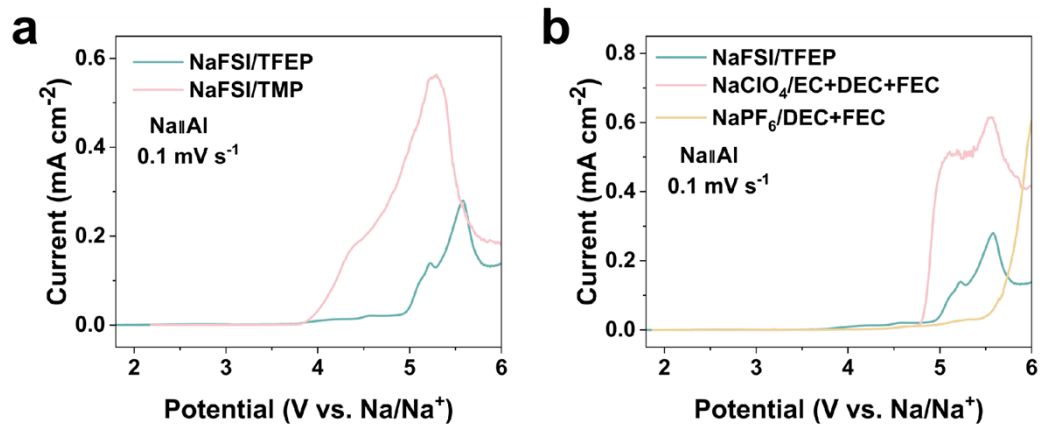

Fig. S2 LSV curves of Na/Al half-cells in different electrolytes with the scan speed rate of 0.1 mV s^{-1} (NaFSI in TMP/TFEP with a concentration of 0.92 M, NaPF$_6$/NaClO$_4$ in electrolytes with a concentration of 1 M)
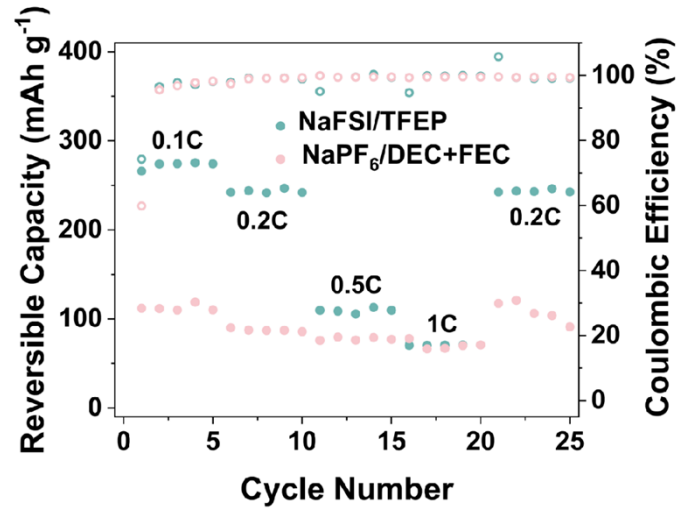
Fig. S3 Rate performances of Na/HC batteries in NaFSI/TFEP and NaPF$_6$/DEC+FEC from the rate of 0.1 C to 1 C.
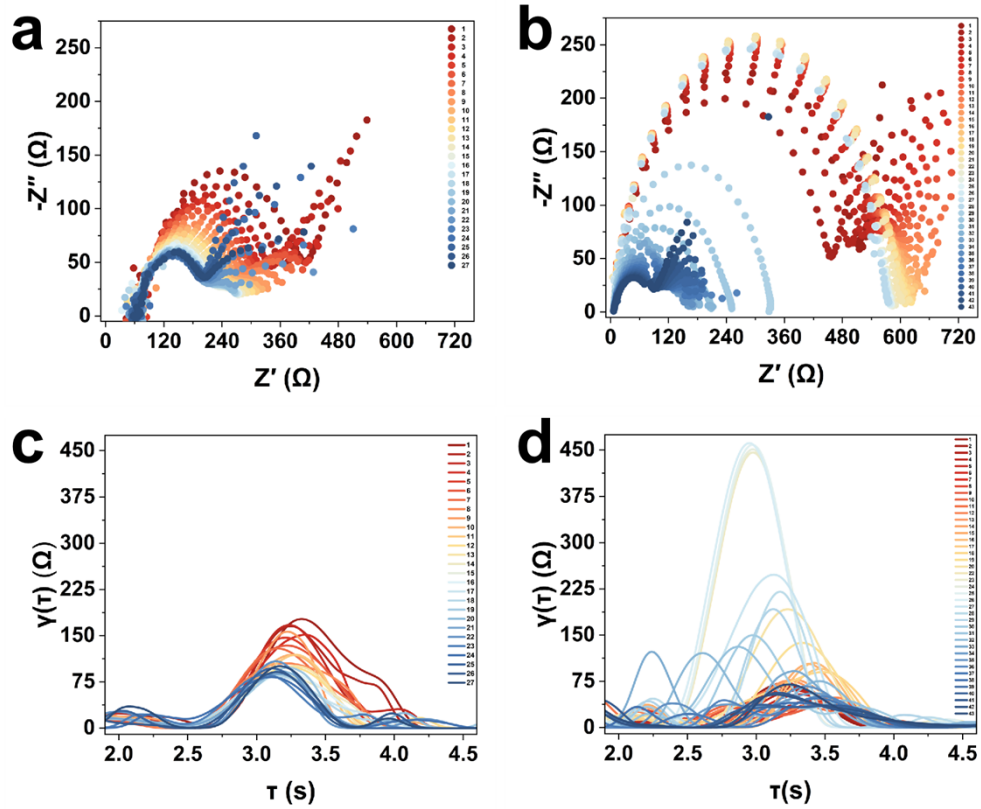

Fig. S4 (a, b) The Nyquist plots and (c, d) the corresponding 2D DRT images of the in-situ EIS tests ($10^5 \sim 1$ Hz) during 1st and 2nd cycling processes of Na/HC half-cells based on (a, c) NaFSI/TFEP and (b, d) NaPF$_6$/DEC+FEC.
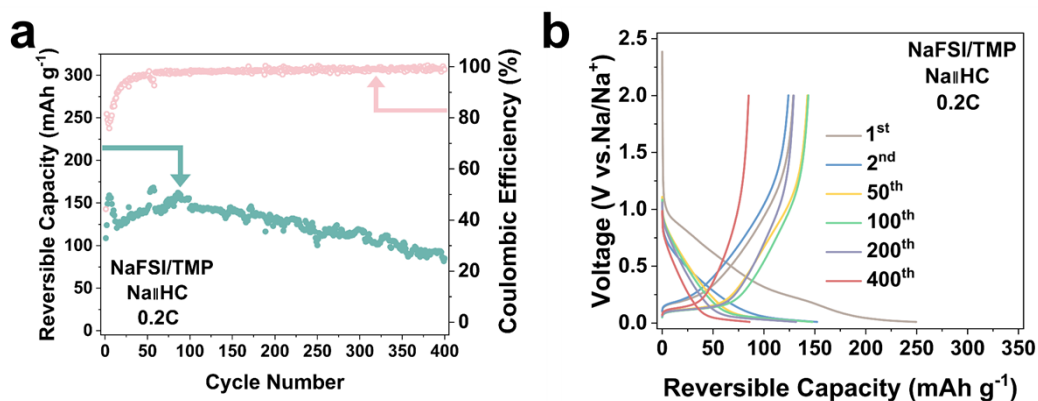
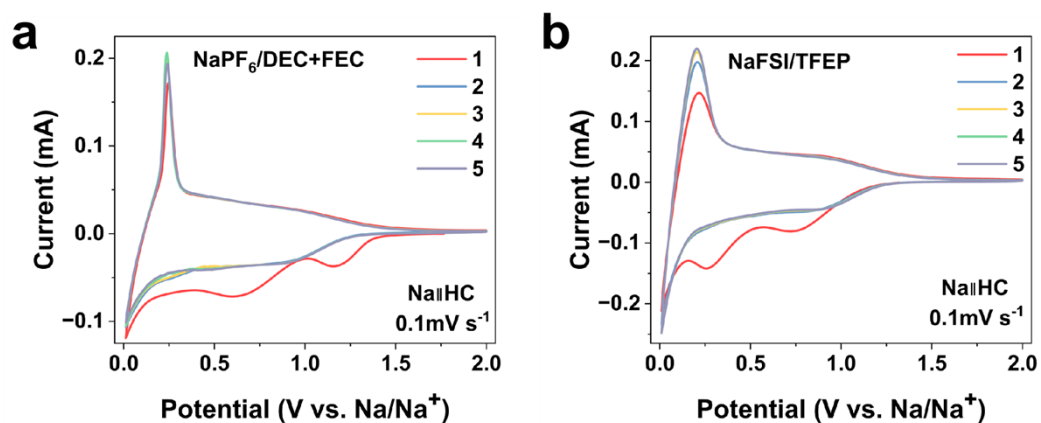**Fig. S5** (a) Cycling performances and (b) voltage profiles at specific cycles of Na/HC half-cells in NaFSI/TMP.

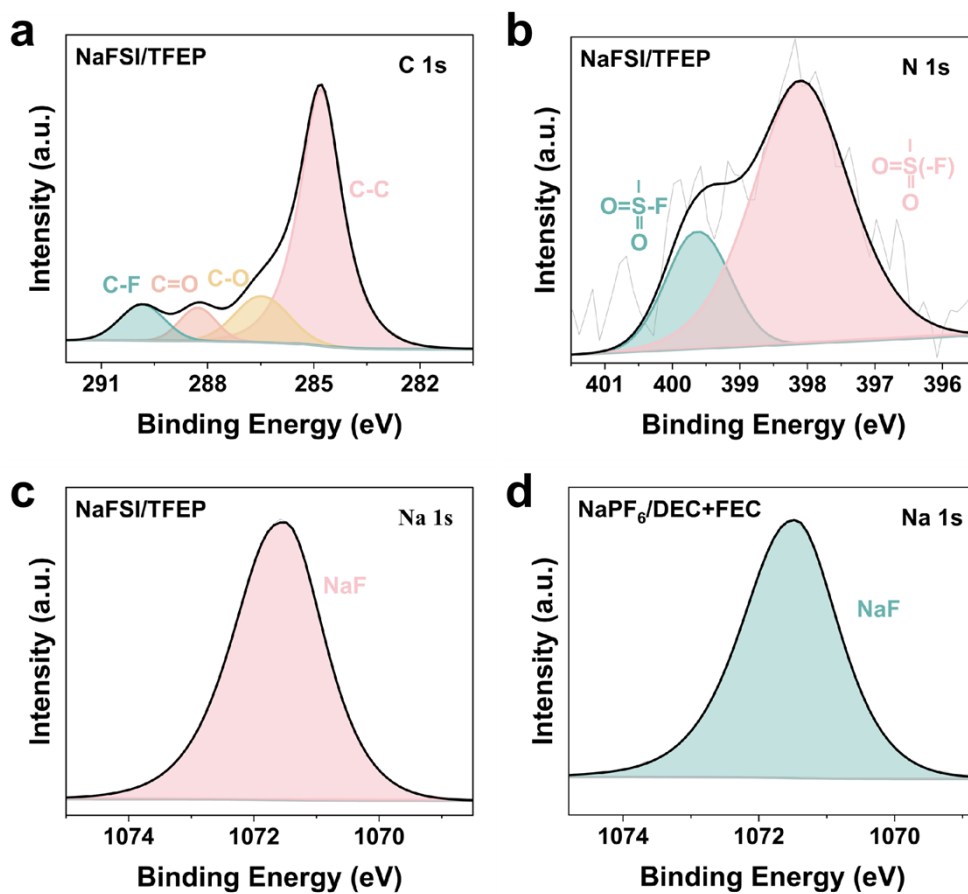**Fig. S6** CV curves of Na/HC half-cells in different electrolytes with the scan rate of 0.1 mV s^{-1}.

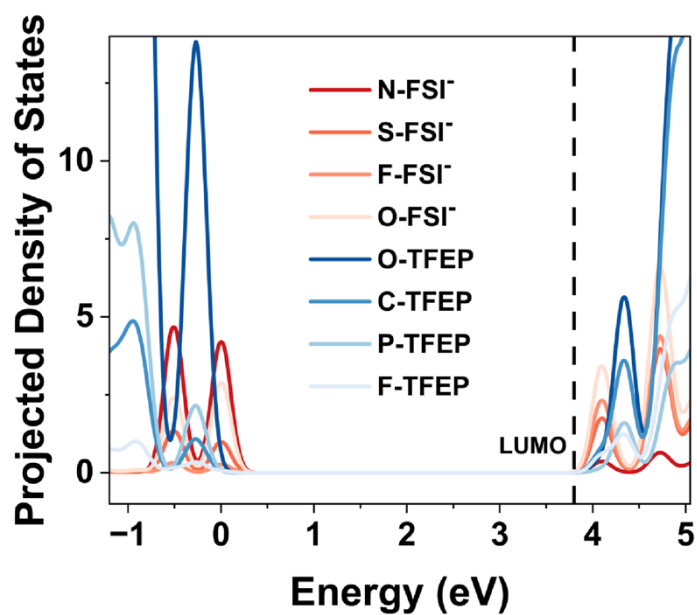**Fig. S7** XPS spectra of cycled HC electrodes with the electrolytes of NaFSI/TFEP (a, b, c) and NaPF$_6$/DEC+FEC (d).

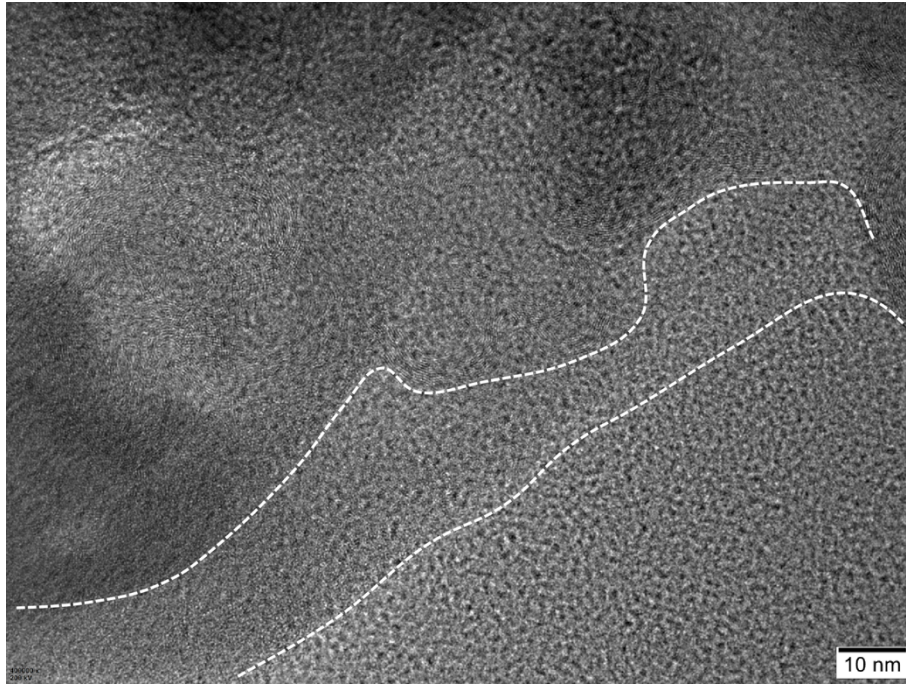**Fig. S8** The original high-resolution image of Figure 4g.

10 nm

Fig. S9 The original high-resolution image of Figure 4i.

Table S1 Summary of the state-of-art HC anodes for SIBs based on different nonflammable electrolytes.

Electrolyte recipe	Initial Coulombic efficiency	Reversible capacity	Cycling performance	Ref
0.9 M NaFSI /TFEP	75.4%	239 mAh g^{-1} @ 50 mA g^{-1}	91.8 % retention after 100 cycles at 50 mA g^{-1}	[10]
NaFSI/DMC-TFP (1.5:1.5:2 in mole)	~76.0%	250 mAh g^{-1} @ 0.1C (1C=300 mAh g^{-1})	-	[11]
NaFSI/TEP-TTE (1:1.5:2 in mole)	~81.0%	247.9 mAh g^{-1}	94.8% retention after 500 cycles	[12]
2.5 M NaClO$_4$ /TMP+5 vol% FEC	67.1%	256.1 mAh g^{-1} @ 20 mA g^{-1}	84 % retention after 1500 cycles at 200 mA g^{-1}	[13]
3.3 M NaFSA/TMP	~73.0%	~250 mAh g^{-1} @ 50 mA g^{-1}	92 % retention after 1200 cycles at 0.2C	[14]
NaTFSI/TMP (1:2 in mole)	71%	245 mAh g^{-1} @ 20 mA g^{-1}	86.6 % retention after 300 cycles at 100 mA g^{-1}	[15]
0.92 M NaFSI/TMP	44.25%	108 mAh g^{-1} @ 0.2C	77% retention after 400 cycles at 0.2C	This work
NaFSI/TFEP (1:5 in mole)	70.8%	246.6 mAh g^{-1} @ 0.2C (1C=279 mAh g^{-1})	100% retention after 400 cycles at 0.2C	

Reference

1   T. H. Wan, M. Saccoccio, C. Chen and F. Ciucci, *Electrochim. Acta*, 2015, **184**, 483-499.

2   X. Zhou, Q. Zhang, Z. Zhu, Y. Cai, H. Li and F. Li, *Angew. Chem. Int. Ed. Engl.*, 2022, **61**, e202205045.

3   B. Delley, *J. Chem. Phys.*, 1990, **92**, 508.

4   B. Delley, *J. Chem. Phys.*, 2000, **113**, 7756.

5   P. Hohenberg, W. Kohn, *Phys. Rev.*,1964, **136**, B864–B871.

6   Y. Zhao, D. G. Truhlar, Theor. Chem., *Acc.*, 2008, **120**, 215–241.

7   Gaussian 16, Revision A.03, Frisch, M. J., Trucks, G. W., Schlegel, H. B., Scuseria, G. E., Robb, M. A., Cheeseman, J. R., Scalmani, G., Barone, V., Petersson, G. A., Nakatsuji, H., Li, X., Caricato, M., Marenich, A. V., Bloino, J., Janesko, B. G., Gomperts, R., Mennucci, B., Hratchian, H. P., Ortiz, J. V., Izmaylov, A. F., Sonnenberg, J. L., Williams-Young, D., Ding, F., Lipparini, F., Egidi, F., Goings, J., Peng, B., Petrone, A., Henderson, T., Ranasinghe, D., Zakrzewski, V. G., Gao, J., Rega, N., Zheng, G., Liang, W., Hada, M., Ehara, M., Toyota, K., Fukuda, R., Hasegawa, J., Ishida, M., Nakajima, T., Honda, Y., Kitao, O., Nakai, H., Vreven, T., Throssell, K., Montgomery, J. A., Jr., Peralta, J. E., Ogliaro, F., Bearpark, M. J., Heyd, J. J., Brothers, E. N., Kudin, K. N., Staroverov, V. N., Keith, T. A., Kobayashi, R., Normand, J., Raghavachari, K., Rendell, A. P., Burant, J. C., Iyengar, S. S., Tomasi, J., Cossi, M., Millam, J. M., Klene, M., Adamo, C., Cammi, R., Ochterski, J. W., Martin, R. L., Morokuma, K., Farkas, O., Foresman, J. B., Fox, D. J. Gaussian, Inc., Wallingford CT, 2016.

8   Tian Lu, Feiwu Chen, *J. Comput. Chem.*, 2012, **33**, 580-592.

9   Tian Lu, Feiwu Chen, *J. Mol. Graph. Model.*, 2012, **38**, 314-323.

10 X. Jiang, X. Liu, Z. Zeng, L. Xiao, X. Ai, H. Yang and Y. Cao, *iScience*, 2018, **10**, 114-122.

11 Y. Jin, P. M. L. Le, P. Gao, Y. Xu, B. Xiao, M. H. Engelhard, X. Cao, T. D. Vo, J. Hu, L. Zhong, B. E. Matthews, R. Yi, C. Wang, X. Li, J. Liu and J.G. Zhang, *Nat. Energy*, 2022, **7**, 718-725.

12 Y. Jin, Y. Xu, P. M. L. Le, T. D. Vo, Q. Zhou, X. Qi, M. H. Engelhard, B. E. Matthews, H. Jia, Z. Nie, C. Niu, C. Wang, Y. Hu, H. Pan and J.G. Zhang, *ACS Energy Lett.*, 2020, **5**, 3212-3220.

13 X. Liu, X. Jiang, Z. Zeng, X. Ai, H. Yang, F. Zhong, Y. Xia and Y. Cao, *ACS Appl. Mater. Inter.*, 2018, **10**, 38141-38150.

14 J. Wang, Y. Yamada, K. Sodeyama, E. Watanabe, K. Takada, Y. Tateyama and A. Yamada, *Nat. Energy*, 2017, **3**, 22-29.

15 X. Jiang, X. Liu, Z. Zeng, L. Xiao, X. Ai, H. Yang and Y. Cao, *Adv. Energy Mater.*, 2018, **8**, 1802176.